ELSEVIER

Marine Geology 180 (2002) 249–270

MARINE GEOLOGY
INTERNATIONAL JOURNAL OF MARINE GEOLOGY, GEOCHEMISTRY AND GEOPHYSICS

www.elsevier.com/locate/margeo

Geochemical evidence for variations in delivery and deposition of sediment in Pleistocene light–dark color cycles under the Benguela Current Upwelling System

Rebecca S. Robinson [a,*], Philip A. Meyers [a], Richard W. Murray [b]

[a] *Department of Geological Sciences, University of Michigan, Ann Arbor, MI 48109, USA*
[b] *Department of Earth Sciences, Boston University, Boston, MA, USA*

Received 28 June 2000; received in revised form 19 March 2001; accepted 25 May 2001

Abstract

Distinctive light–dark color cycles in sediment beneath the Benguela Current Upwelling System indicate repetitive alternations in sediment delivery and deposition. Geochemical proxies for paleoproductivity and for depositional conditions were employed to investigate the paleoceanographic processes involved in creating these cycles in three mid-Pleistocene intervals from ODP Sites 1082 and 1084. Concentrations of total organic carbon (TOC) vary between 3.5 and 17.1%. Concentrations of $CaCO_3$ vary inversely to TOC and Al, which suggests that both carbonate dissolution and terrigenous dilution contribute to the light–dark cycles. Opal concentrations are independent of both TOC and $CaCO_3$, therefore eliminating diatom production and lateral transport of shelf material as causes of the light–dark cycles. $\delta^{13}C_{org}$ and $\delta^{15}N_{tot}$ values do not vary across light–dark sediment intervals, implying that the extent of relative nutrient utilization did not change. The stable $\delta^{15}N_{tot}$ values represent a balanced change in nitrate supply and export production and therefore indicate that productivity was elevated during deposition of the TOC-rich layers. Parallel changes in concentrations of indicator trace elements and TOC imply that changes in organic matter delivery influenced geochemical processes on the seafloor by controlling consumption of pore water oxygen. Cu, Ni, and Zn are enriched in the darker sediment as a consequence of greater organic matter delivery. Redox-sensitive metals vary due to loss (Mn and Ba) or enrichment (Mo) under reducing conditions created by TOC oxidation. Organic matter delivery impacts subsequent geochemical changes such as carbonate dissolution, sulfate reduction and the concentration of metals. Thus, export production is considered ultimately responsible for the generation of the color cycles.

Keywords: Benguela; organic carbon; carbonate; $\delta^{15}N$; trace elements; paleoproductivity

1. Introduction

The Benguela Current Upwelling System (BCUS) is one of the most productive regions of the world's oceans. Sediments beneath the upwelling zones are rich in total organic carbon (TOC) with concentrations that range from 2 to 20%

* Corresponding author. Present address: Princeton Environmental Institute, M30 Guyot Hall, Princeton University, Princeton, NJ 08544, USA. Fax: +1-609-258-1712.
E-mail addresses: rebeccar@princeton.edu (R.S. Robinson), pameyers@umich.edu (P.A. Meyers), rickm@bu.edu (R.W. Murray).

0025-3227/02/$ – see front matter
PII: S0025-3227(01)00217-1

(Berger et al., 1998). The concentration of sedimentary TOC has been used to approximate past primary productivity at the ocean surface (Müller and Suess, 1979; Sarnthein et al., 1988; Stein et al., 1989). Given concentrations far above the global average for deep-sea sediments (0.2%) (Degens and Mopper, 1976), the general relation between elevations in seafloor TOC and surface productivity seems to be true for the BCUS. However, the TOC levels along the southeast African margin vary dramatically in patterns that do not seem to be linked directly to other estimates of paleoproductivity (Bertrand et al., 2000; Berger et al., 1998; Diester-Haass et al., 1986; Meyers, 1984; Summerhayes et al., 1995). The variations are associated with obvious light–dark color cycles (Berger et al., 1998; Gardner et al., 1984) that suggest major periodic changes in the system. These changes could be due to climate and its effect on surface currents and productivity, they could result from fluctuations in the regional water mass structure, or they could reflect other cyclical processes, such as sea level changes.

Results from three scientific drilling cruises – DSDP Legs 40 and 75 and ODP Leg 175 – have provided important information about the history of the Benguela Current. The high productivity associated with the BCUS originated in the late Miocene ($\sim$10 Ma) and has intensified through time (Meyers, 1984; Seisser, 1980). Sediment records from DSDP Site 532 on the Walvis Ridge contain color cycles that reveal high amplitude variations in organic carbon and carbonate concentrations and accumulation (Diester-Haass et al., 1986; Gardner et al., 1984; Meyers, 1984). Gardner et al. (1984) demonstrated that the carbonate and organic carbon variations do not correspond exactly and hence concluded that dilution by non-carbonate sediment components rather than carbonate dissolution controlled the color cycles at intervals of 40–60 kyr. In contrast, Diester-Haass and coworkers (1986) used the sand-size fraction in cycles from near the Pliocene–Pleistocene boundary to deduce that organic carbon maxima correspond to minima in opal and $CaCO_3$ concentrations. Using opal abundance as the main productivity proxy, they inferred significant dissolution of carbonate in the dark sediment layers. Moreover, they postulated that the light–dark cyclicity was related to glacial–interglacial sea level changes.

In many parts of the BCUS record, intervals of elevated TOC evidently resulted from resuspension of shelf sediments and their subsequent redeposition on the slope, rather than simply from paleoproductivity changes in directly overlying waters (Diester-Haass et al., 1986; Summerhayes et al., 1995). This process is common on passive margins. Diester-Haass et al. (1986) presented a model in which glacial intervals at Site 532 were accompanied by redeposition of organic carbon-rich sediments from the shelf and resulting increased dissolution of carbonate on the slope, whereas interglacial intervals contained records of higher production in overlying waters. In support of this hypothesis, Summerhayes et al. (1995) documented glacial–interglacial changes in organic carbon concentrations and used ^{14}C dating to confirm that the dark intervals of marine oxygen isotope stages 2 and 4 resulted from sediment resuspension and redeposition. Interestingly, the organic carbon-rich dark interval deposited during stage 3 did not contain evidence of reworking (Summerhayes et al., 1995).

Opal accumulations in sediment have been widely employed as a paleoproductivity proxy (Diester-Haass et al., 1986; Lange et al., 1999; Leinen et al., 1986; Lyle et al., 1988; Rea et al., 1991; Verardo and McIntyre, 1994). However, this parameter may not be the best indicator of primary production on the Namibian margin (Summerhayes et al., 1995). Since the early Pleistocene, the opal content in slope sediment has progressively decreased, but marine production has remained high (Berger et al., 1998). Opal-producing diatoms and radiolarians are found at present in the region of high production over the shelf. Offshore, the relatively high production is dominated primarily by coccolithophores rather than diatoms.

Summerhayes et al. (1995), noting potential problems with opal as well as documenting mixing and redeposition of organic carbon, suggested that there is no single reliable productivity proxy for the region. They therefore used a combination

of organic carbon and opal mass accumulation rates as the most viable productivity proxy (Summerhayes et al., 1995). For the late Pleistocene, they estimated that productivity varied over precessional (20 kyr) time periods due to changes in trade wind strength, with maxima during stages 3 and 5. Furthermore, they concluded that overall upwelling intensified during glacial times in the latest Pleistocene. In contrast, opal contents alone led Diester-Haass et al. (1986) to postulate that production near the Pliocene–Pleistocene boundary varied at glacial–interglacial (40 kyr) intervals and was higher during interglacial times.

Given the number of interpretations for their origins, the light–dark intervals remain paleoceanographic puzzles that require new approaches to help understand their cause and significance. Specifically, what is the evidence for episodic or cyclical changes in paleoceanographic parameters such as productivity, dissolution of carbonate, and delivery of non-carbonate sediment components? Furthermore, changes in the burial rates of inorganic and organic carbon have implications for the region's role in the global carbon cycle. Production may have been enhanced by more vigorous upwelling and thus may indicate a stronger biological pump (Broecker, 1982), or perhaps bottom water conditions changed and carbon burial was more efficient. The present study utilizes multiple geochemical proxies to evaluate the roles of productivity, organic matter preservation, and carbonate dissolution in formation of light–dark color cycles in Pleistocene sediment sequences from ODP Sites 1082 and 1084.

2. Sampling and analysis

2.1. Setting

The Benguela Current is the eastern boundary current of the south Atlantic subtropical gyre and flows towards the equator about 300 km offshore of the coast of southwest Africa, splitting into the Benguela Coastal Current (BCC) and Benguela Oceanic Current (BOC) north of 28°S (Fig. 1). South-southeasterly winds drive upwelling of cold, nutrient-rich waters from 200–500 m water depth (Lutjeharms and Meeuwis, 1987). Several upwelling cells exist along the southwest African coast, with the strongest being the Lüderitz Cell at 25°S adjacent to ODP Site 1084 (Fig. 1). The Walvis Bay Cell is the closest to ODP Site 1082, and it is slightly weaker than the Lüderitz cell (Lutjeharms and Meeuwis, 1987). Primary production is highest over the continental shelf region, within the BCC. Eddies and filaments of nutrient-rich water carry the pockets of high productivity water offshore over much of the slope region underlying the BOC. Production over the slope is enhanced additionally by a shelf-edge upwelling system that lies within the BOC (Summerhayes et al., 1995).

2.2. Samples and age estimates

Samples from three sediment sequences that contain light–dark–light cycles were selected during ODP Leg 175 from Holes 1082A and 1084A. Sites 1082 and 1084 are located on the continental slope (Fig. 1) in 1280 and 1992 m water depth respectively. Although seaward of the main upwelling, the core locations contain records of the upwelling history because of the filaments of high productivity water that reach them (Wefer et al., 1998). Sample depths are given in meters composite core depth (mcd), which are based on a continuous sediment column synthesized from the multiple holes at each site (Wefer et al., 1998). Age estimates were made based on the shipboard biostratigraphy (Wefer et al., 1998), which has been verified by subsequent oxygen isotope stratigraphy (L. Vidal, personal communication). The 50–75 mcd (45–64 mbsf) interval from Site 1082A represents approximately 0.59–0.90 Ma. The 142–148 mcd (123–127 mbsf) interval of Site 1084A is 0.73–0.78 Ma, and the 240–248 mcd (211–219 mbsf) interval spans about 1.09–1.15 Ma.

2.3. Analytical strategies and procedures

Concentrations of the three principal biogenic components of sediment – $CaCO_3$, TOC, and opal – were used to evaluate changes in biogenic sedimentation and paleoproductivity. Samples were first freeze-dried and then powdered. $CaCO_3$

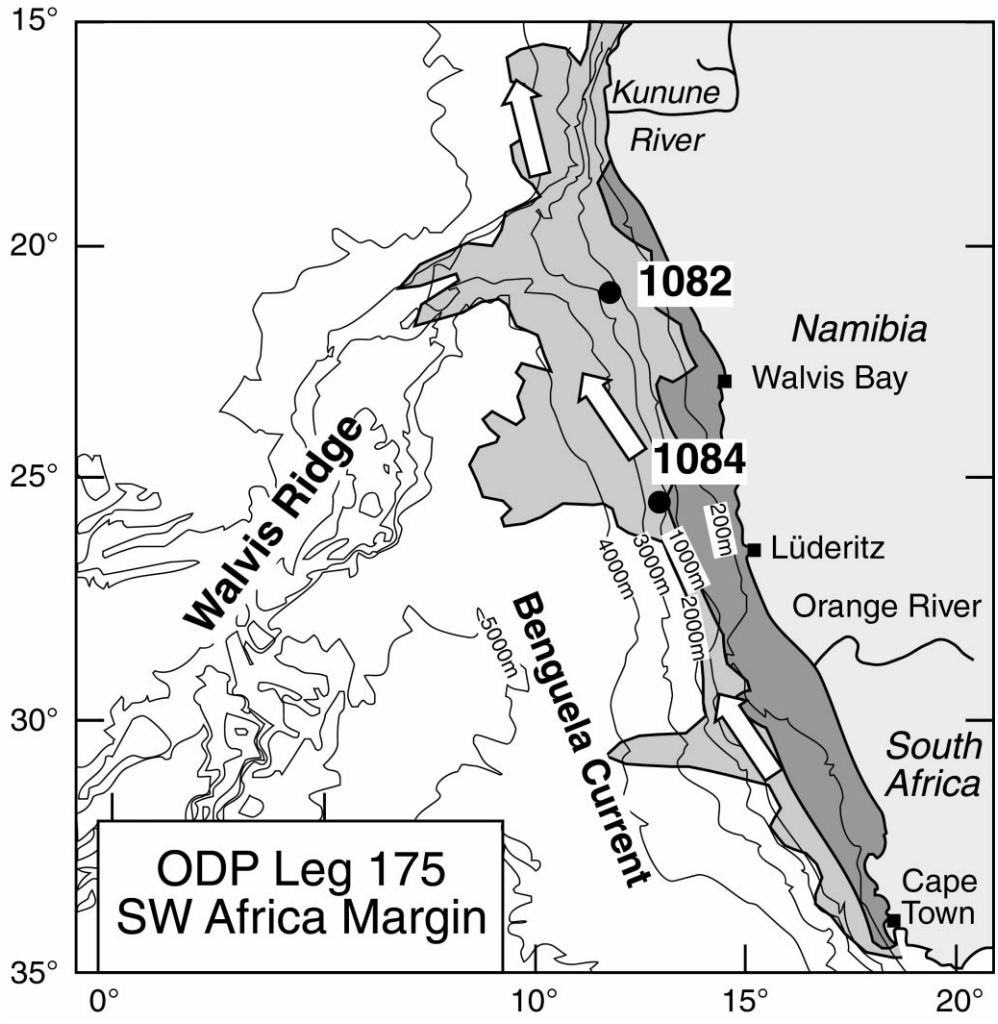

Fig. 1. Locations of ODP Sites 1082 and 1084 relative to the general axis of the Benguela Current (bold arrow). Areas of perennial and periodic upwelling as defined by Lutjeharms and Stockton (1987) are shown by dark and light shading, respectively.

concentrations were measured using a simple carbonate bomb technique (Müller and Gastner, 1971) in which powdered bulk sediment was reacted with 3 N HCl. The volume of CO_2 released was measured and related to the volume of CO_2 produced by a known mass of pure $CaCO_3$. Analytical precision as relative standard deviation (RSD) is 2% and analytical accuracy was within precision. The carbonate-free residue was rinsed with distilled de-ionized water and used for subsequent analyses of C and N elemental and stable isotope compositions. Concentrations of TOC and total residual nitrogen (TN) were measured using a Carlo Erba 1108 CNHS-O elemental analyzer. TOC and TN concentrations are reported on a whole sediment basis, each with absolute precision better than 0.05% (1σ). Accuracy, determined by comparison with a reference standard (Buffalo River sediment), was within precision. Atomic organic carbon/residual nitrogen (C/N) values were calculated from the TOC and TN concentrations and used as proxies of organic matter origin and alteration. Concentrations of opal in sub-samples of the powdered bulk sedi-

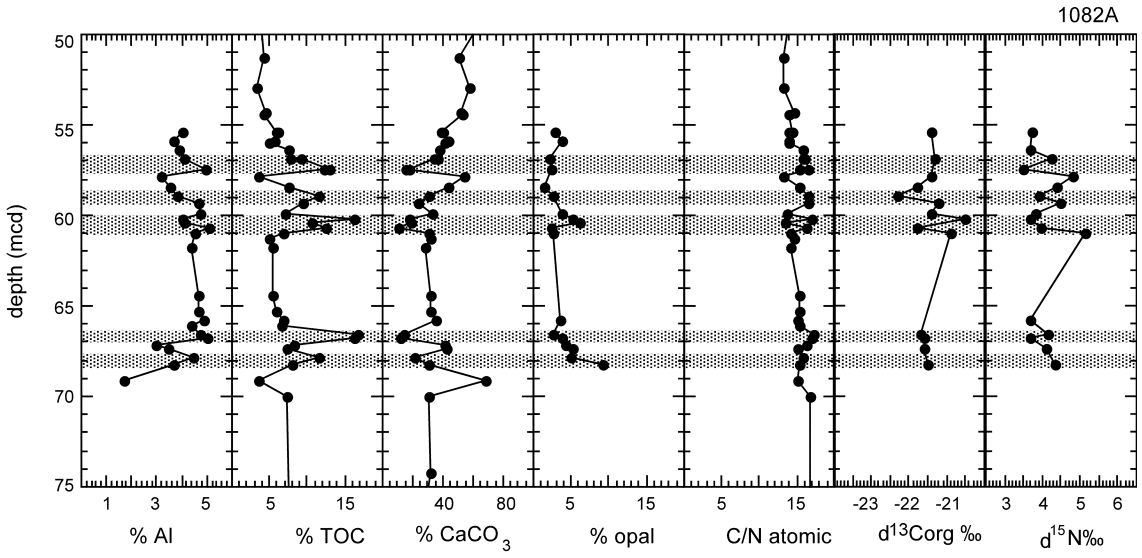

Fig. 2. Concentrations (wt%) of Al, TOC, $CaCO_3$, and opal. TOC C/N atomic values, and $\delta^{13}C_{org}$ ‰ and $\delta^{15}N_{tot}$ ‰ through several light–dark intervals from Cores 1082A-6+7. The depth (mcd) interval ranges in age from approximately 0.6 to 0.9 Ma with an average sedimentation rate of ~8 cm/kyr.

ment were determined following the wet leaching and spectrophotometric analysis technique of Mortlock and Froelich (1989), with precision of ~10% (RSD) as a result of the very low opal concentrations. Accuracy was determined through measurement of an Indian Ocean reference sediment and was within analytical precision.

The carbon and nitrogen stable isotope compositions of sedimentary organic matter were used as proxies of past nutrient sources and rates of or-

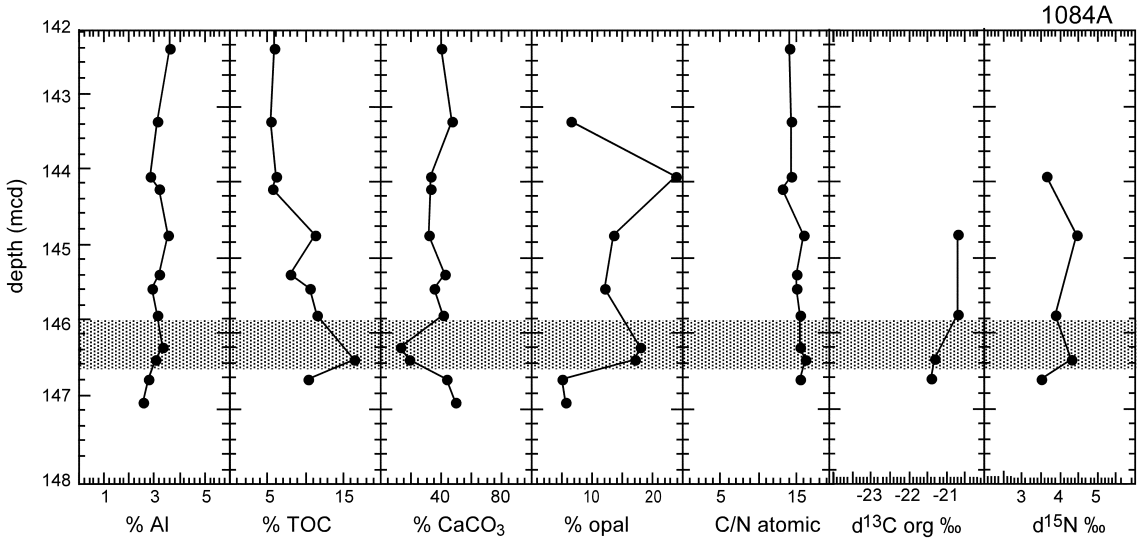

Fig. 3. Concentrations (wt%) of Al, TOC, $CaCO_3$, and opal. TOC C/N atomic values, and $\delta^{13}C_{org}$ ‰ and $\delta^{15}N_{tot}$ ‰ through a light–dark–light interval from Cores 1084A-14+15. This depth interval ranges in age from 0.7 to 0.8 Ma with an average sedimentation rate of ~14 cm/kyr. Organic carbon and opal concentrations are higher than in the 1082 interval.

ganic matter production. Carbonate-free sediment residues were combusted in sealed Vycor tubing in the presence of CuO and Cu at 800°C. The ratio of $^{13}C/^{12}C$ in the resulting CO_2 was measured relative to the NBS-20 standard using a VG Isogas Prism mass spectrometer following removal of H_2O and NO_x. Organic $\delta^{13}C$ values are reported relative to PDB standard with an analytical precision of ± 0.1‰. Nitrogen gas was isolated cryogenically and trapped in a bulb on clean silica gel for immediate analysis of its $^{15}N/^{14}N$ ratio. Residual $\delta^{15}N$ values are reported as ‰ values relative to air with variability ± 0.2‰.

Selected trace elements in the bulk sediment were measured. Mo, Mn, Zn, Ni, Cu, Ba, and P concentrations are used here as potential inorganic productivity proxies and/or to estimate bottom water chemistry changes. Approximately 0.12 g of freeze-dried and powdered sample was dissolved by microwave digestion and a series of dissolution and evaporation steps involving HNO_3, HF, $HClO_4$, HCl, and H_2O_2, following a procedure similar to that of Murray and Leinen (1996) and Yarincik et al. (2000a). Once the samples were completely digested, solutions were diluted 100- and 1000-fold for trace and major element analyses, respectively, using a Jobin Yvon JY 138 Ultrace inductively coupled plasma emission spectrometer (ICP-ES) in the Analytical Geochemistry Laboratory at Boston University. Samples were prepared and analyzed in random depth order. Analytical precision (RSD) was better than 2% for all concentrations and ratios. A standard reference sediment (BCSS-1) was analyzed to confirm analytical accuracy. Accuracy of the measurements was within precision, although accuracy for Mo could not be checked since the concentration of Mo in BCSS-1 is less than the 3 ppm (Yarincik et al., 2000a,b) detection limit of the ICP-ES.

3. Results and discussion

3.1. Origin of color cycles

3.1.1. Terrigenous inputs

Inasmuch as Gardner et al. (1984) concluded that the light–dark cycles present at Site 532 originated from variations in delivery of terrigenous sediment, evaluation of this possibility at Sites 1082 and 1084 was one of our first priorities. Alu-

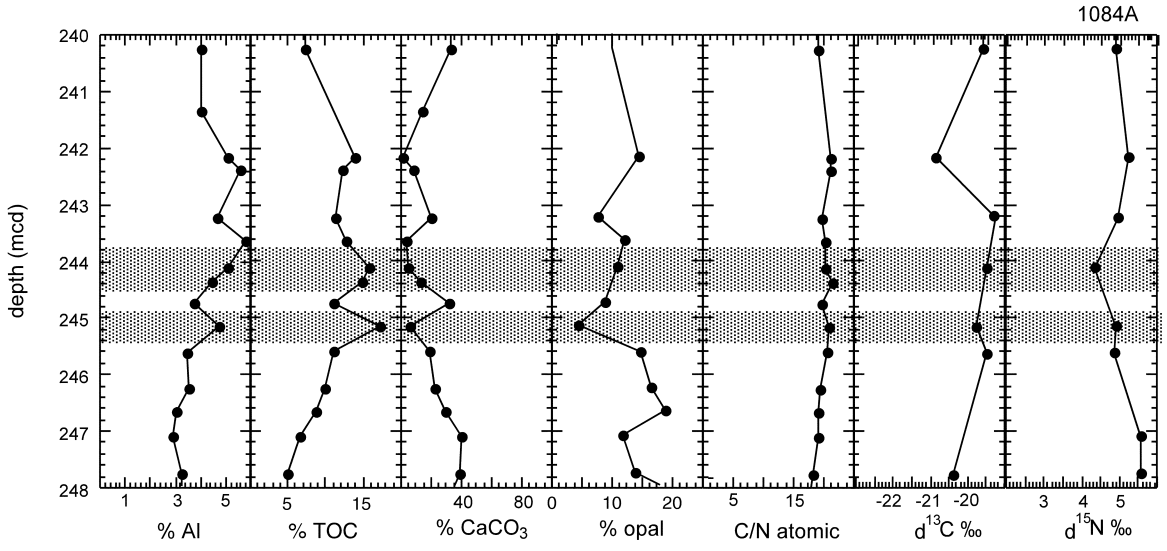

Fig. 4. Concentrations (wt%) of Al, TOC, $CaCO_3$, and opal. TOC C/N atomic values, and $\delta^{13}C_{org}$ ‰ and $\delta^{15}N_{tot}$ ‰ through another light–dark interval from Cores 1084A-25+26. This older interval ranges in age from 1.06 to 1.17 Ma and has a sedimentation rate of ~25 cm/kyr. The overall higher % TOC, % opal and $\delta^{13}C$ and $\delta^{15}N$ values suggest that paleoproductivity was greater at 1.1 Ma over Site 1084.

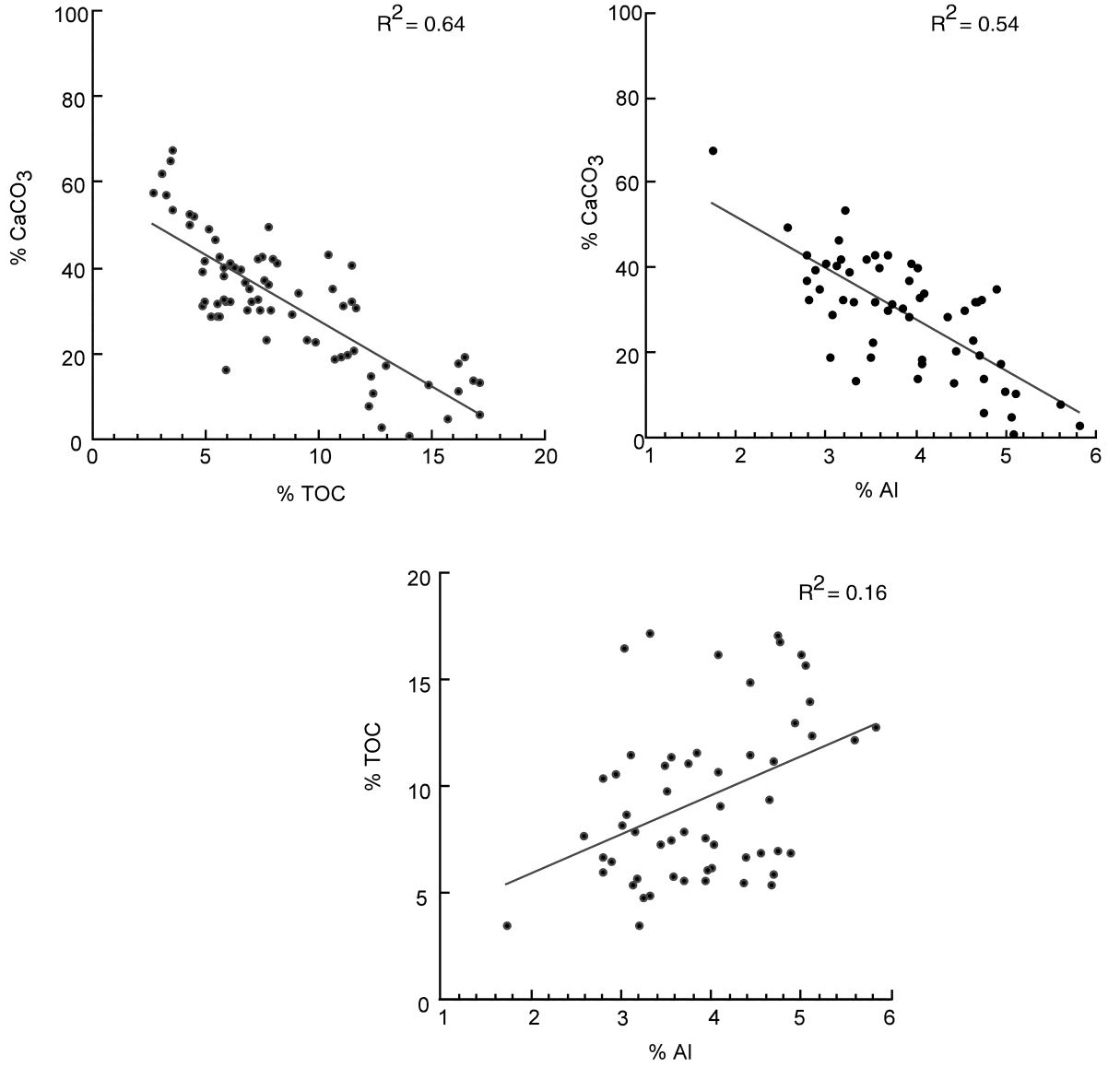

Fig. 5. A negative relation between TOC and $CaCO_3$ and a weaker negative relation between $CaCO_3$ and Al suggest that both dilution and dissolution are contributing to the formation of the light–dark cycles. TOC and Al show no significant relationship. Data from Sites 1082 and 1084 are combined.

minum concentrations are commonly used as a proxy for contents of clay minerals derived from continental weathering (Piper and Isaacs, 1995; Schroeder et al., 1997). Although excess Al can be used as an indicator of export production in certain low terrigenous flux environments (Murray et al., 1993; Murray and Leinen, 1996), the terrigenous supply overwhelms the excess scavenged Al even in organic-rich continental margin settings (e.g. Yarincik et al., 2000a). Accordingly, we use the concentration of Al as an indicator of terrigenous material in the BCUS slope sediments. Al concentrations for the three time intervals that we studied do not systematically vary with organ-

Table 1
TOC, $CaCO_3$ and opal concentrations, C/N values, and organic matter $\delta^{13}C$ and $\delta^{15}N$ values for sediment samples from ODP Holes 1082A and 1084A

Core-section interval	Composite depth (m)	$CaCO_3$ (%)	TOC (%)	C/N atomic	Opal (%)	$\delta^{15}N$ air (‰)	$\delta^{13}C$ PDB (‰)
Hole 1082A							
6H-4 10–12	55.41	40.3	6.2	13.9	2.9	3.2	−21.4
6H-4 62–64	55.93	43.0	5.6	14.0	3.7		
6H-4 65–66	55.96	41.7	4.9	13.9			
6H-4 110–111	56.41	37.1	7.6	15.9		3.2	
6H-5 7–8	56.88	36.3	7.7	16.1			
6H-5 10–12	56.91	34.3	9.1	15.7	2.1	3.7	−21.3
6H-5 62–64	57.43	17.6	13.0	15.2	2.5	3.0	
6H-5 65–66	57.46	15.2	12.3	16.6			
6H-5 104–105	57.85	54.0	3.5	13.3		4.3	−21.4
6H-6 10–12	58.41	43.0	7.5	15.4	1.4	3.9	−21.8
6H-6 62–64	58.96	30.9	11.6	16.6	2.6	3.4	−22.3
6H-6 100–101	59.31	23.4	9.4	16.5		4.0	−21.2
6H-7 10–12	59.91	32.6	7.0	13.7	3.8	3.3	−21.4
6H-7 43–45	60.24	17.8	16.2	16.9	5.3	3.2	−20.5
6H-7 60–61	60.41	18.7	10.7	13.4	6.2		
6H-7 90–92	60.71	10.9	12.4	16.2	2.5	3.4	−21.8
6H-7 120–122	61.01	30.4	6.9	14.1	2.7	4.7	−20.9
7H-1 9–10	61.30	31.3	4.9	14.5			
7H-1 56–57	61.77	28.8	5.5	14.2			
7H-3 23–24	64.44	32.0	5.5	15.3			
7H-3 104–105	65.25	32.3	5.9	15.4			
7H-4 10–12	65.81	35.4	6.9	15.0	3.7	3.2	
7H-4 39–40	66.10		6.7	15.2			
7H-4 82–84	66.53	13.9	16.8	17.2	2.5	3.6	−21.7
7H-4 104–106	66.75	11.2	16.2	16.9	3.8	3.2	−21.6
7H-4 143–145	67.15	41.3	8.2	16.3	4.3		
7H-5 10–12	67.31	42.2	7.3	15.1	5.1	3.6	−21.6
7H-5 62–64	67.83	20.7	11.5	15.7	5.5		
7H-5 104–106	68.25	30.2	7.9	15.2	9.2	3.8	−21.5
7H-6 45–46	69.16	67.9	3.6	15.1			
7H-6 129–130	70.00	30.4	7.3	16.6			
Hole 1084A							
14H-4 143–145	143.20	46.9	5.4	14.3	6.5		
14H-5 65–67	143.92	32.6	6.0	14.5	23.8	3.7	
14H-5 83–84	144.10	32.7	5.8	13.1			
14H-5 142–144	144.71	32.3	11.4	15.9	13.5	4.5	−20.7
14H-6 46–47	145.23	42.4	7.9	15.1			
14H-6 65–67	145.42	35.1	10.6	15.1	12.0		
14H-6 99–101	145.76	40.6	11.5	15.6		3.9	−20.7
14H-6 142–144	146.19	13.4	17.4	15.6	18.0		
14H-7 9–11	146.36	19.4	16.5	16.3	17.1	4.3	−21.3
14H-7 34–36	146.61	43.1	10.4	15.4	4.9	3.5	−21.4
14H-7 65–67	146.92	49.9	11.6	15.3	5.5		
15H-2 46–47	151.17	37.0	6.7	15.0		4.6	−20.9
15H-4 46–47	154.17	41.1	6.1	14.6			
25X-1 85–87	240.25	33.1	7.3	14.5	9.0	4.8	−19.7
25X-2 125–127	242.15	1.0	13.9	16.1	13.5	5.2	−21.0
25X-2 148–149	242.38	8.0	12.2	16.4			
25X-3 84–86	243.24	19.8	11.2	15.0	6.7	4.9	−19.4
25X-3 125–127	243.65	3.1	12.8	15.4	11.2		

Table 1 (*continued*)

Core-section interval	Composite depth (m)	$CaCO_3$ (%)	TOC (%)	C/N atomic	Opal (%)	$\delta^{15}N$ air (‰)	δ13C PDB (‰)
25X-4 20–22	244.10	5.0	15.7	15.6	10.0	4.3	−19.6
25X-4 46–47	244.36	13.1	14.9	16.4			
25X-4 85–87	244.75	31.5	11.1	15.1	7.8		
25X-4 125–127	245.15	6.2	17.1	16.0	3.4	4.8	−19.9
25X-5 20–22	245.60	19.3	11.0	15.7	13.9	4.8	−19.6
25X-5 85–87	246.25	22.7	9.8	14.9	15.5		
25X-5 125–127	246.65	29.4	8.8	14.5	18.0		
25X-6 20–22	247.10	40.0	6.5	14.6	10.9	5.5	
25X-6 85–87	247.75	39.1	4.8	13.8	13.0	5.5	−20.5
25X-6 125–127	248.15	32.4	4.9	13.2	20.5		
26X-2 46–47	251.06	16.3	5.9	12.3			

Sample depths are given in mcd, derived by splicing together the depths below seafloor of the multiple holes drilled at both of these sites (Wefer et al., 1998).

ic matter concentrations in the light–dark cycles, but they have a negative relationship with $CaCO_3$ (Figs. 2–5). The correspondence of low $CaCO_3$ and higher Al concentrations in the dark layers suggests that fluctuations in dilution by terrigenous materials may be important in creating the color cycles in these Pleistocene sediment intervals.

3.1.2. Carbonate and organic carbon

TOC and $CaCO_3$ concentrations vary with sediment color in the studied intervals. Moreover, the two biogenic components are strongly inversely related (Figs. 2–5). Dark sediment layers have notably high TOC concentrations, generally greater than 10%, and their $CaCO_3$ concentrations range between 11 and 40%. In contrast, TOC concentrations range between 2 and 10% in the light layers, where $CaCO_3$ concentrations are 30–68%. All of these sediment sequences, and especially the dark layers, are markedly enriched in organic carbon relative to the global deep-sea sediment average of 0.2% TOC (Degens and Mopper, 1976; McIver, 1975). The abundant availability of readily oxidizable organic matter favors production of large amounts of CO_2 at the seafloor at or soon after the time of sediment deposition. The subsequent increase in CO_2 concentration in bottom waters and pore waters enhances dissolution of $CaCO_3$ (Berger, 1970; Emerson and Bender, 1981). The inverse relation between TOC and $CaCO_3$ concentrations consequently implies that variations in delivery of reactive organic matter that led to variations in the amount of carbonate dissolution were also involved in creating the distinct light–dark color cycles. Without mass accumulation rates we cannot quantitatively evaluate the relative importance of dissolution and dilution in the Benguela system. Nonetheless, we suggest that both are contributing to the $CaCO_3$ signal.

The variations in delivery of organic matter implied by the light–dark cycles can occur in several ways. One possibility is that the variations in the concentrations may record cyclical strengthening and weakening of paleoproductivity in the entire BCUS (Diester-Haass et al., 1986). Another is that the positions of the areas of more elevated surface productivity may have fluctuated over time, sometimes being over Sites 1082 and 1084 and sometimes being some distance from them (Diester-Haass et al., 1986). Finally, delivery of organic matter from overlying waters may have been augmented by lateral contributions, most likely as downslope redeposition of TOC-rich sediment from areas of higher productivity on the continental shelf or along the shelf-edge (Diester-Haass et al., 1986; Summerhayes et al., 1995). Delivery of organic matter that could be easily oxidized and thereby lead to dissolution of $CaCO_3$ at the seafloor would vary as a result of any of these processes.

3.1.3. Biogenic opal

Opal concentrations are ~3–4% through the

interval from Hole 1082, with two small peaks above 5% (Fig. 2 and Table 1). The upper peak at 60 mcd corresponds to a peak in TOC while the lower one falls in a TOC low. Opal concentrations in the two intervals from Hole 1084A are generally higher and more variable, ranging from 3.4 to 23.8%. (Figs. 3 and 4). These variations are not systematically related to TOC changes. It is important to keep in mind that opal is not considered to be a useful indicator of productivity in BCUS slope sediment since the opal production is mainly restricted to the waters overlying the shelf and since preservation is almost certainly variable and poor.

3.1.4. Organic $\delta^{13}C$ values

Organic $\delta^{13}C$ values range narrowly from -19.7 to -22.3‰ and are typical of marine organic matter (e.g. Meyers, 1994). There is little variation in $\delta^{13}C_{org}$ values through the light–dark sequences. In the interval from Hole 1082A, where there are obvious 0.5–1‰ shifts, the changes have no systematic relation to the light–dark color cycles. Both the minimum (-22.3‰) and the maximum (-20.5‰) in the Hole 1082A samples are associated with organic-rich dark intervals. $\delta^{13}C_{org}$ values in the younger depth interval of 1084 range narrowly between -20.7 and -21.4‰ (Fig. 3), while in the older 1084 interval they are $\sim$1‰ higher and range from -19.7 to -21.0‰ (Fig. 4). Absence of change in $\delta^{13}C_{org}$ values across the light–dark intervals suggests that the availability of dissolved inorganic carbon to primary producers remained relatively stable during deposition of both the light and dark intervals and that growth rate, cell size effects, and other variables that affect $\delta^{13}C_{org}$ had limited influence.

3.1.5. C_{org}/N_{tot} values

Organic C/N values in the Site 1082 interval vary between 14 and 17 (Fig. 2). Higher C/N values correlate with greater TOC concentrations ($r^2 = 0.52$, $n = 73$). The C/N values in the two Site 1084 intervals vary narrowly between 15 and 16 (Figs. 3 and 4). These atomic ratios are intermediate between unaltered algal organic matter (5–8) and fresh land plant material (20–35) (Emerson and Hedges, 1988; Meyers, 1994). However, it is unlikely that these C/N values record a mixture of marine and terrestrial plant organic material because the adjacent Namib Desert is a poor source for significant contributions of land-derived organic matter. Furthermore, shipboard Rock-Eval analyses show the organic matter to be type II (Wefer et al., 1998), which is derived principally from algae. Instead, the elevated C/N values and shifts associated with higher TOC concentrations are probably a consequence of enhanced sedimentation of marine organic matter and are not reliable indicators of organic matter source in these settings.

C/N values that are elevated above algal values are common in organic carbon-rich marine sediment (Meyers, 1997). They evidently result from the selective loss of N as organic matter settles from the photic zone. With high organic matter fluxes, more labile, nitrogen-bearing proteins are selectively decomposed relative to other organic matter components such as carbohydrates and lipids (Verardo and McIntyre, 1994). Benthic chamber experiments have documented a preferential degradation of nitrogen-rich organic material resulting in a sedimentary C/N ratio of 10–16 and pore water ratio of 5 ± 2 (Hammond et al., 1999). This type of preferential N depletion and consequent relative C enrichment is recognized in other organic carbon-rich sediment, such as the Mediterranean Sea (Meyers and Doose, 1999; Nijenhuis and Lange, 2000), light–dark color cycles from DSDP Site 532 (Meyers, 1984), the equatorial Atlantic (Verardo and McIntyre, 1994), and the NW Mexican slope (Ganeshram et al., 1999). In organic carbon-poor sediments, it appears that degradation has proceeded beyond the more labile nitrogenous components and thus a lower C/N value is preserved. C/N elevations are most pronounced when TOC concentrations are highest, suggesting that a higher rate of organic matter delivery leads to reduced relative degradation.

3.1.6. $\delta^{15}N$ values

At Site 1082, $\delta^{15}N_{tot}$ values average $\sim$3.5‰ with small amplitude variations between 3.2 and 4.7 (Fig. 2). Lower $\delta^{15}N_{tot}$ values correlate with higher TOC concentrations. In the 1084 intervals

there is almost no variation despite the high amplitude TOC and $CaCO_3$ concentration changes (Figs. 3 and 4). The $\delta^{15}N_{tot}$ record of the 240–248 mcd interval of 1084A is also ~1.5‰ heavier overall with values ranging from 4.3 to 5.5‰ (Fig. 4).

Nitrogen isotope compositions of sediment organic matter can be affected by denitrification in the water column (Altabet et al., 1995; Ganeshram et al., 1995, 1999), nitrogen fixation by cyanobacteria in the water column (Haug et al., 1998), inputs from land, variable preservation (Sachs and Repeta, 1999), and the relative degree of nitrate utilization by algae (Altabet and Francois, 1994). Studies measuring $\delta^{15}N_{tot}$ in the Benguela region are limited, but there is evidence that sedimentary $\delta^{15}N_{tot}$ primarily reflects relative nitrate utilization in this area (Holmes et al., 1996, 1998). The main regional productivity maxima lie over the shelf, and they correspond to the highest nitrate concentrations in the surface waters as well as to low $\delta^{15}N_{tot}$ values and high TOC in the surface sediment (Holmes et al., 1998). At present, the upwelling core over the shelf supplies more nitrate to the surface than is utilized. The abundance of nitrate permits greater discrimination in favor of ^{14}N resulting in organic matter bearing a relatively low $\delta^{15}N$ value. Offshore, farther from the upwelling core, nitrate levels are lower and the corresponding surface sediments have higher $\delta^{15}N_{tot}$ values (Holmes et al., 1996, 1998).

Denitrification creates ^{15}N-enriched nitrate through preferential removal of ^{14}N under reducing conditions within the water column and can result in high bulk $\delta^{15}N$ values of ~7–9‰ (Altabet et al., 1995, 1999; Ganeshram et al., 1995). Today, there are three major regions of denitrification, the Eastern Tropical North Pacific offshore of Mexico, the Eastern Tropical South Pacific off Peru, and the Arabian Sea (Altabet et al., 1995, 1999; Ganeshram et al., 1999, 2000; Liu and Kaplan, 1989). There is no evidence for major denitrification within the Benguela region. If the $\delta^{15}N$ of the local nitrate pool in the near surface waters was the result of denitrification during the Pleistocene, the resulting sedimentary $\delta^{15}N_{tot}$ would likely be greater than modern values and not less.

In fact, the $\delta^{15}N_{tot}$ values for all the samples measured are low in comparison to many measured values for marine organic matter (Altabet et al., 1995, 1999; Francois et al., 1992; Ganeshram et al., 1995, 1999; Haug et al., 1998; Kienast, 2000; Rau et al., 1987). Cyanobacteria use atmospheric nitrogen with little or no fractionation to produce organic matter with a $\delta^{15}N_{tot}$ of −1 to +1‰ (Brandes et al., 1998). Thus, contributions of organic matter resulting from nitrogen fixation could result in low values such as we see here. However, nitrogen fixation is uncommon in nutrient-replete systems (Haug et al., 1998; Rau et al., 1987). Moreover, it is more important where nitrate abundance, relative to P, is reduced due to denitrification (Haug et al., 1998).

Alteration of organic matter during very early diagenesis at or near the sediment water interface generally creates a 2–5‰ increase in $\delta^{15}N_{tot}$ between settling material and surface sediments in deep waters, while preserving the pattern of $\delta^{15}N_{tot}$ distribution (Altabet et al., 1995). In organic carbon-rich continental margin sediments, however, there seems to be little or no diagenetic effect on $\delta^{15}N_{tot}$ (Ganeshram et al., 2000; Altabet et al., 1999). Given the high concentrations of organic carbon in the light–dark intervals, the relatively low $\delta^{15}N_{tot}$ values observed here probably reflect the original signal without a significant diagenetic overprint. Furthermore, there is no covariation between $\delta^{15}N_{tot}$ and C/N, suggesting that differential alteration between the light and dark intervals is not modifying the $\delta^{15}N_{tot}$ signal.

Resuspension and redeposition of shelf material during low seastands might explain both the enrichment of TOC and the light N isotope signal. Indeed, shelf sediment in the Benguela region is isotopically lighter (Holmes et al., 1998) and richer in both organic carbon and opal (Summerhayes et al., 1995). However, while the organic carbon-rich intervals do bear slightly lower $\delta^{15}N_{tot}$ values at Site 1082, there is no clear relationship between opal and TOC in any of the sampled intervals, which argues against the importation of TOC and isotopically light N (Figs. 2–4).

Alternatively, the TOC-rich intervals may have been deposited when upwelling was more intense. In this scenario, productivity increased but rela-

tive nitrate utilization did not change, implying that nitrate availability also increased. Slightly higher $\delta^{15}N_{tot}$ values correlate with lower TOC concentrations (Figs. 2–4), suggesting that the relative extent of nitrate utilization was greater when TOC inputs were lower. The interpretation that increased upwelling intensity corresponds to an increase in available nitrate and higher TOC fluxes agrees with the interpretation of Brüchert et al. (2000) based on micropaleontologic and chemical data from three dark intervals at Site 1084 from the late Pliocene and Pleistocene.

The concordant offset of $\sim 0.8‰$ in both the $\delta^{13}C_{org}$ and $\delta^{15}N_{tot}$ between Sites 1082 and 1084 likely reflects the present difference in relative nutrient utilization described by Holmes et al. (1998) for the modern BCUS. Site 1084, closer to the Lüderitz upwelling cell, bears overall higher isotope values and higher TOC concentrations and at present is considered to be in a more productive region of the upwelling system than near Site 1082. Extrapolating this into the past, it appears that Site 1084 had higher export production than Site 1082. There is an additional 0.5‰ offset between the lower (1.1 Ma) and upper (0.7 Ma) intervals at Site 1084 (Figs. 2–4). Based on the isotope values alone, with higher values at 1.1 Ma, one could reason that the relative nutrient utilization was greater at 1.1 due to a decrease in upwelling rather than an increase in export production at this site. Assuming that basin-scale changes in the balance between nitrogen fixation and denitrification did not change the $\delta^{15}N$ of the source nitrate and taking the isotope values in conjunction with the higher TOC and opal concentrations, we infer that export production was enhanced at 1.1 Ma and relative nutrient utilization was higher.

3.2. Elemental indicators of changes in sediment delivery and depositional conditions

The source composition of continental sediment components is assessed here by comparing concentration of Ti, which is strongly associated with continental detritus to Ti values established for average shale (Table 2). Ti vs. Al cross-plots from our samples were compared to the Ti vs. Al plots from published average shale values to determine the closest approximation of terrigenous source contributions. We utilized Archean Mudstone (Taylor and McLennan, 1985) as our approximation of terrigenous contributions to the Benguela sediments. Differences in the slope of Ti vs. Al cross-plots from our samples when compared to Archean Mudstone reveal that the terrigenous fractions of our samples are not similar in composition to Post-Archean Average Shale (PAAS), the most commonly utilized terrigenous source approximation. In order to observe the variation from the lithogenic fraction in the Namibian margin sediment, excess amounts of each element were estimated relative to Archean Mudstone (Table 3):

$$El_{xs} = El_t - Al_t \times (El_{A.M.}/Al_{A.M.})$$

where El_{xs} is element excess, El_t is the total measured and $El_{A.M.}$ is the published Archean Mudstone value. We will express El_{xs} as a percent of E_t:

$$= (El_{xs}/El_t) \times 100$$

Table 2
Average concentrations of trace elements in Post-Archean Average Shale (PAAS) and Archean Mudstone (Taylor and McLennan, 1985) and organic matter (Collier and Edmond, 1984) used as guidelines for evaluating enrichment in the sediment

Element	PAAS (element/Al)	Archean Mudstone (element/Al)	Plankton (element/Al)
Ba	0.0065	0.0064	80
Cu	0.0005	0.0017	11
Mn	0.0085	0.0075	–
Mo	0.00001	0.00001	2
Ni	0.0005	0.0011	7.5
P	0.0070	–	–
Zn	0.0008	–	110

There are no published values for P or Zn for Archean Mudstone so we calculated their excess based on the PAAS (Taylor and McLennan, 1985). Use of the different source approximation as a normalizing agent changes only the absolute value of the calculated excess and not the relative patterns of change.

3.2.1. Organic matter delivery of trace metals

'Excess' contributions of elements to sediments beyond those contributed by the terrigenous fraction can come from sources such as seawater or plankton. Relative metal abundances are reported as element/Al ratios here to minimize the effects of any variations in terrigenous inputs. Zn/Al, Ni/Al, and Cu/Al profiles parallel TOC/Al (Figs. 6–8). Zn, Ni, and Cu are enriched in plankton and delivered to the seafloor with organic matter (Brumsack, 1986; Calvert and Price, 1970; Collier and Edmond, 1984). Maxima in the element/Al profiles correspond to those in the TOC/Al record. Cross-plots of Zn/Al, Ni/Al, and Cu/Al versus % TOC demonstrate the highest correlation relative to other elements and maintain a moderate enrichment above lithogenic contributions (Fig. 9). Calculated excesses are only 5–10 times what is estimated from organic matter delivery (Tables 2 and 3). Downcore variations in Zn, Ni, and Cu might reflect changes in organic matter delivery rates. However, there is potential for diagenetic alteration of the metal concentrations after deposition. Francois (1988) documented Ni and Cu are more susceptible to enrichment under suboxic to anoxic conditions than Zn, but this relation is not apparent in sediments from our light–dark intervals.

3.2.2. Trace metal indicators of redox conditions

Mn is depleted in BCUS sediment relative to Archean Mudstone (Fig. 9). Under oxic conditions, bulk Mn concentrations are elevated above crustal values (Calvert and Pedersen, 1994; Dickens and Owen, 1994). The Mn/Al ratio in Archean Mudstone is 0.008 and the highest ratio value measured here is 0.0027. The low Mn/Al values observed in this study are probably caused by the well-known Mn^{2+} loss that follows depletion of oxygen in the surface sediment pore water (Crusius et al., 1996; Dickens and Owen, 1994; Morford and Emerson, 1999; Thamdrup et al., 1994; Yarincik et al., 2000b).

Mo is strongly enriched relative to the Archean Mudstone; excess Mo is 98–99% of the total Mo measured (Table 3, Fig. 9). Mo/Al is in excess of lithogenic values throughout the three sampling intervals, and the Mo/Al maxima correlate to peaks in the other metals and TOC. There is very little Mo in terrigenous or planktonic detritus (Brumsack, 1986; Collier and Edmond, 1984), so the enrichment must be from another source such as seawater.

Excess Mo values are all greater than 20 ppm, more than 10 times what plankton could have contributed to the sediment. Mo enrichment is associated with highly reducing conditions in the water column or sediment pore waters (Crusius et al., 1996; Morford and Emerson, 1999; Yarincik et al., 2000b). There is also evidence for the incorporation of reduced MoO_2^+ into the humic fraction of organic matter (Francois, 1988). Mo at MoO_4^{2-} is approximately conservative in seawater and not highly enriched in terrigenous materials. MoO_4^{2-} is transformed to MoS_4^{2-} in the presence of HS^- (Helz et al., 1996), which is readily scavenged by Fe and humic substances (Erickson and Helz, 2000; Helz et al., 1996). Mo enrichment is thus a highly sensitive indicator of sulfate-reducing conditions. However, the bottom waters were not anoxic at Sites 1082 and 1084; the sediment is bioturbated throughout the intervals and contains benthic foraminifers (Brüchert et al., 2000; Wefer et al., 1998). Sulfate-reducing conditions must have been met at or just below the sediment–water interface where the Mo concentration gradient between seawater and depleted pore waters is greatest. Erickson and Helz (2000) suggest that this situation is ideal for Mo scavenging because NH_4^+ acts as a catalyst for the molybdate transformation while seawater acts as a steady supplier of Mo. Increases in Mo/Al values can consequently be interpreted as times of enhanced organic matter oxidation when sulfate reduction and the resulting increase in HS^- concentration occurred at a shallow subbottom depth (Erickson and Helz, 2000) (Figs. 6–8).

Table 3
Elemental concentrations and calculated trace element excess for individual sediment samples

Core-section interval	Depth	Mo	% xs	Zn	% xs	Ni	% xs	Mn	% ex	Ba	% xs	Cu	% xs	P	% xs	Al	Ti	Fe
		(ppm)		(ppm)		(ppm)		(ppm)		(ppm)		(ppm)		(ppm)		(%)	(%)	(%)
Hole 1082A																		
6H-4 10–12	55.41	23	98	88	61	54	18	87	−243	904	72	47	57	716	61	4.00	0.22	2.65
6H-4 62–64	55.93	26	98	78	60	55	26	75	−266	787	70	44	58	795	68	3.69	0.20	2.62
6H-4 110–111	56.41	24	98	97	66	66	35	70	−317	814	69	55	65	816	67	3.91	0.21	2.49
6H-5 10–12	56.91	23	98	93	63	75	40	83	−267	821	68	61	66	831	66	4.08	0.24	2.91
6H-5 65–66	57.43	39	99	151	72	117	53	111	−231	1061	71	103	76	1071	68	4.93	0.29	3.35
6H-5 104–106	57.85	20	98	60	55	51	31	47	−408	745	73	40	60	704	68	3.20	0.15	2.04
6H-6 10–12	58.41	20	98	87	65	61	36	72	−266	796	72	50	65	758	67	3.54	0.21	2.38
6H-6 62–64	58.96	33	99	104	69	88	52	81	−253	901	73	77	75	942	72	3.84	0.22	2.47
6H-6 100–101	59.31	31	98	121	68	94	45	114	−203	968	70	73	68	1008	68	4.63	0.28	3.40
6H-7 10–12	59.91	46	99	107	63	93	44	117	−201	813	63	75	68	939	65	4.72	0.27	3.42
6H-7 43–45	60.24	44	99	140	75	114	61	95	−219	366	30	97	79	1272	78	4.06	0.23	2.71
6H-7 60–61	60.41	30	99	122	72	99	55	102	−197	978	74	92	78	1161	76	4.07	0.24	3.07
6H-7 90–92	60.71	35	98	130	67	126	55	140	−172	294	−10	96	73	1654	78	5.10	0.33	3.97
6H-7 120–122	61.01	31	98	147	74	85	41	101	−235	822	65	62	63	1437	78	4.54	0.27	3.11
7H-1 56–57	61.77	24	98	81	54	53	9	97	−235	712	61	41	48	1829	83	4.35	0.26	3.38
7H-3 23–24	64.44	26	98	83	52	54	5	101	−243	794	63	48	51	639	49	4.65	0.25	2.82
7H-3 104–105	65.25	31	98	124	68	61	15	91	−283	861	66	49	53	692	53	4.67	0.24	2.82
7H-4 10–12	65.81	36	99	107	61	90	40	117	−211	928	67	73	67	900	62	4.88	0.27	3.13
7H-4 39–40	66.10	32	99	82	54	66	26	99	−230	827	66	54	59	804	62	4.38	0.23	2.64
7H-4 82–84	66.53	48	99	129	69	109	52	104	−241	293	−3	107	78	958	65	4.75	0.26	2.80
7H-4 104–106	66.75	53	99	153	72	111	50	107	−248	446	29	99	75	978	64	4.99	0.27	3.06
7H-4 143–145	67.15	21	98	83	69	63	48	50	−346	783	76	51	71	784	73	2.99	0.17	1.95
7H-5 10–12	67.31	21	98	80	64	67	43	76	−237	801	73	55	69	834	71	3.43	0.20	2.42
7H-5 62–64	67.83	36	99	112	66	91	46	114	−190	820	66	73	70	859	64	4.43	0.24	3.07
7H-5 104–106	68.25	22	98	84	63	64	36	77	−256	784	70	56	67	757	66	3.68	0.21	2.21
7H-6 45–46	69.16	13	99	51	71	42	54	7	−1742	811	86	29	70	680	82	1.73	0.10	1.00
Hole 1084A																		
14H-2 46–47	139.23	18	98	87	62	51	15	79	−270	725	66	52	62	739	63	3.92	0.20	2.56
14H-4 46–47	142.23	15	97	78	61	52	24	63	−323	863	74	53	66	816	69	3.58	0.18	2.11
14H-4 143–145	143.20	11	97	70	62	44	22	53	−339	833	76	48	67	810	73	3.12	0.16	2.07
14H-5 65–67	143.92	13	98	73	67	55	44	41	−409	825	78	48	71	695	72	2.80	0.14	1.81
14H-5 83–84	144.10	14	97	81	66	55	36	53	−347	817	75	56	71	756	71	3.18	0.16	2.08
14H-5 142–144	144.71	18	98	96	69	69	43	54	−390	788	71	80	78	881	72	3.55	0.18	2.08
14H-6 46–47	145.23	18	98	87	69	66	48	46	−410	875	77	76	79	872	75	3.14	0.15	1.72
14H-6 65–67	145.42	27	99	121	79	80	59	39	−460	896	79	86	83	930	78	2.93	0.14	1.81
14H-6 99–101	145.76	3	88	15	−74	9	−284	–	–	817	76	7	−127	78	−179	3.10	0.02	1.48
14H-6 142–144	146.19	46	99	162	83	112	67	42	−490	353	40	118	86	943	75	3.32	0.16	2.12
14H-7 9–11	146.36	36	99	135	81	92	63	41	−452	1138	83	103	85	901	76	3.04	0.16	1.98

Table 3 (*continued*)

Core-section interval	Depth	Mo	% xs	Zn	% xs	Ni	% xs	Mn	% ex	Ba	% xs	Cu	% xs	P	% xs	Al	Ti	Fe
		(ppm)		(ppm)		(ppm)		(ppm)		(ppm)		(ppm)		(ppm)		(%)	(%)	(%)
14H-7 34–36	146.61	21	98	106	78	70	56	39	−432	953	81	89	84	877	78	2.78	0.14	1.67
14H-7 65–67	146.92	17	98	87	75	68	58	33	−480	909	82	75	83	822	78	2.57	0.13	1.51
15H-2 46–47	151.17	14	98	78	70	59	48	43	−382	723	76	66	79	783	75	2.78	0.14	1.67
15H-4 46–47	154.17	12	96	87	62	58	25	80	−268	832	70	64	69	843	67	3.95	0.20	2.41
25X-1 85–87	240.25	21	98	92	63	57	22	90	−234	1145	78	65	69	869	68	4.03	0.19	2.37
25X-2 46–47	241.36	33	99	129	74	95	53	92	−225	307	17	94	79	1033	73	4.01	0.21	2.84
25X-2 125–127	242.15	29	98	160	73	120	53	100	−278	499	35	125	80	1448	76	5.07	0.27	3.25
25X-2 148–149	242.38	21	97	158	70	116	47	132	−216	265	−34	130	78	1715	77	5.59	0.29	3.69
25X-3 84–86	243.24	24	98	135	70	111	53	107	−227	678	56	118	80	1279	74	4.69	0.25	3.15
25X-3 125–127	243.65	22	97	163	70	119	46	136	−219	526	30	131	78	1505	73	5.81	0.29	3.34
25X-4 20–22	244.10	23	98	175	76	142	61	123	−206	418	23	156	84	1250	72	5.05	0.27	3.33
25X-4 46–47	244.36	35	99	172	78	148	67	93	−254	317	12	169	87	1230	75	4.41	0.23	2.78
25X-4 85–87	244.75	27	98	133	76	109	62	72	−286	816	71	120	84	1268	79	3.73	0.19	2.26
25X-4 125–127	245.15	35	98	195	79	176	70	92	−284	208	−45	138	83	1402	76	4.74	0.23	3.09
25X-5 20–22	245.60	27	99	122	76	108	64	76	−242	968	77	88	80	1213	80	3.49	0.18	2.65
25X-5 85–87	246.25	24	98	115	74	104	63	75	−248	474	53	92	81	1101	78	3.50	0.17	2.33
25X-5 125–127	246.65	22	98	107	76	92	64	68	−234	1070	82	82	81	1189	82	3.05	0.16	2.14
25X-6 20–22	247.10	26	99	88	72	71	55	65	−230	1106	83	71	80	1060	81	2.88	0.15	1.88
25X-6 85–87	247.75	18	98	79	65	60	40	68	−256	1054	80	50	67	832	73	3.25	0.16	1.97
25X-6 125–127	248.15	21	98	79	64	60	39	68	−263	1040	80	46	64	775	70	3.31	0.16	2.06

Sample depths are given in mcd below sea bottom. Excesses were calculated relative to El/Al ratio of Archean Mudstone (Taylor and McLennan, 1985). Data are overspecified for calculation purposes. See text for discussion of true precision. Note that negative excess Ba values are an artifact of assigning Archean Mudstone as the source estimate.

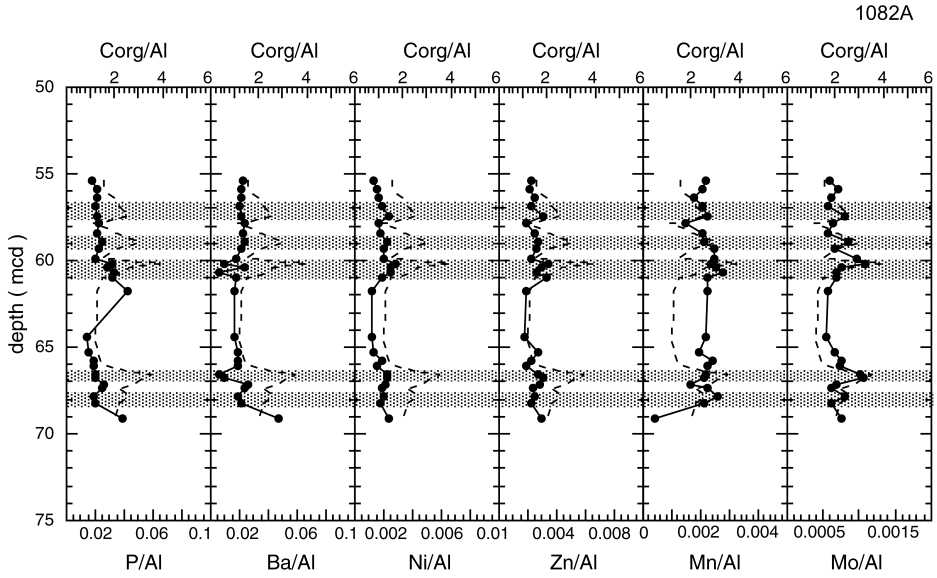

Fig. 6. Downcore element/Al values superimposed on TOC/Al values (dashed line) for reference from Site 1082. Variations in trace element concentrations are occurring with changes in TOC concentration downcore. Depth given in mcd.

3.2.3. Barite delivery and diagenesis

Ba is delivered to the seafloor by two main processes: (1) within the silicate lattice of terrigenous material and (2) in association with organic matter as barite ($BaSO_4$). In most of our samples, Ba/Al ratios are higher than in Archean Mudstone (Fig. 9). This enrichment can be attributed to the delivery of biogenic barite in association with organic matter. However, in organic-rich sediment, Ba/Al values are close to or less than Ba/Al for Archean Mudstone (Figs. 6–9), implying no enrichment.

Under well-oxygenated bottom water conditions, barite is possibly a better recorder of organ-

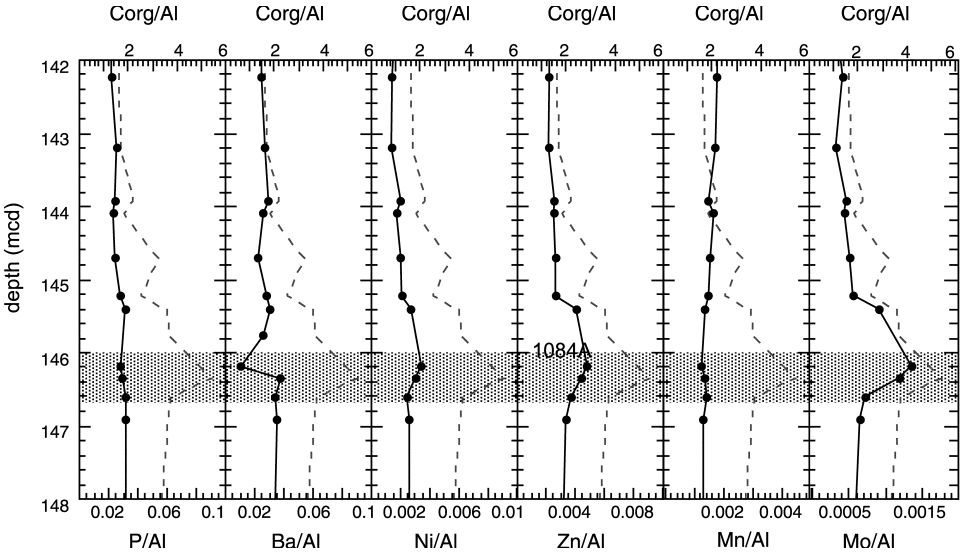

Fig. 7. Downcore element/Al values superimposed on TOC/Al values (dashed line) from Core 1084A-14, 142–147 mcd.

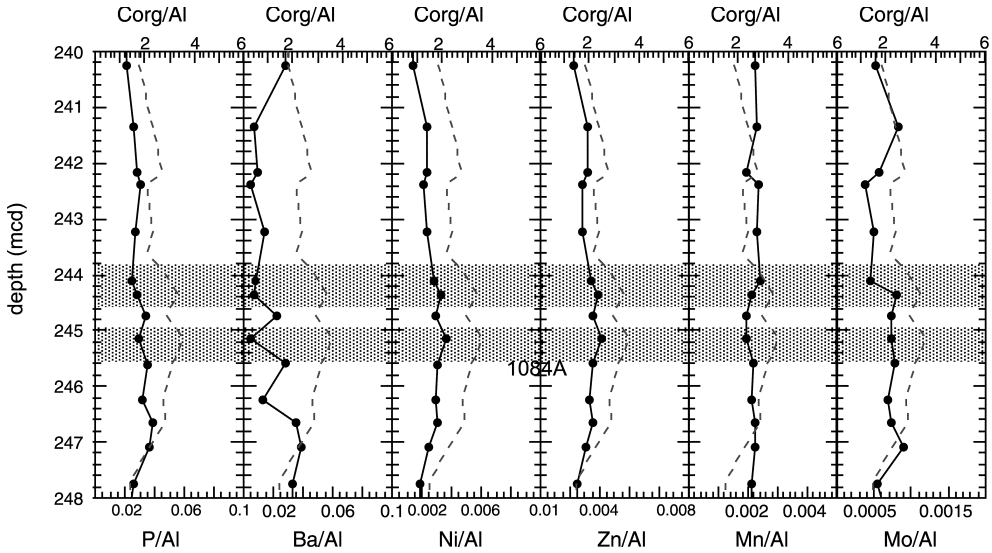

Fig. 8. Downcore element/Al values superimposed on TOC/Al values (dashed line) from Core 1084A-25, 240–248 mcd.

ic matter production than TOC concentrations (Dymond et al., 1992; Schroeder et al., 1997). On the slope of the Namibian margin, where the excess values drop from 70–80% to $<30\%$ of the total, Ba appears to have been remobilized after deposition, probably as a consequence of sulfate reduction and undersaturation of the pore waters with respect to sulfate. The dissolution of $BaSO_4$ could result from high organic matter fluxes under suboxic conditions and not only during sulfate reduction (McManus et al., 1998). In this setting, it seems likely that extremely high organic matter oxidation rates and sulfate-reducing conditions, corresponding to the maxima in TOC concentration, could drive the loss of Ba. This is reinforced by the inverse correlation to Mo/Al, a probable indicator of high sulfate-reducing conditions. The conditions for Ba loss appeared to have been more severe in the intervals that contain the highest organic carbon concentrations (Figs. 6–8).

3.2.4. Phosphorus delivery and diagenesis

Phosphorus is delivered to sediments primarily by organic matter and also incorporated in calcite and apatite. The regeneration of P from sediments is complicated, involving both the oxidation rates of organic carbon, bottom water oxygen concentrations, the depth of O_2 penetration into surface sediments, and the cycling of Fe (Ingall and Jahnke, 1994; McManus et al., 1997). P is released during the oxidation of organic matter. In oxygenated sediments, it is adsorbed by authigenic Fe and Mn oxyhydroxides. Although the P/Al values in our samples are generally in excess of lithogenic contributions (Fig. 9), light–dark sediment intervals show no systematic P/Al patterns (Figs. 6–8). There is obvious regeneration of Mn, thus suggesting that P could not be retained by Mn oxyhydroxides. Organic matter oxidation rates and the depletion of pore water oxygen occurring in both the relatively TOC-poor and TOC-rich intervals suggest that the P/Al profiles reflect diagenesis rather than primary production.

3.3. General discussion

The $\delta^{13}C_{org}$ and $\delta^{15}N$ records suggest that relative nutrient utilization levels were the same despite the markedly different concentrations of organic carbon. Low $\delta^{15}N_{tot}$ values (3–5‰) reflect a relatively constant abundance of available nitrate in the BCUS. The evidence presented by Brüchert et al. (2000) suggests that variations in organic carbon burial relate to upwelling strength. If the difference in the TOC concentration between light and dark intervals reflects changes in

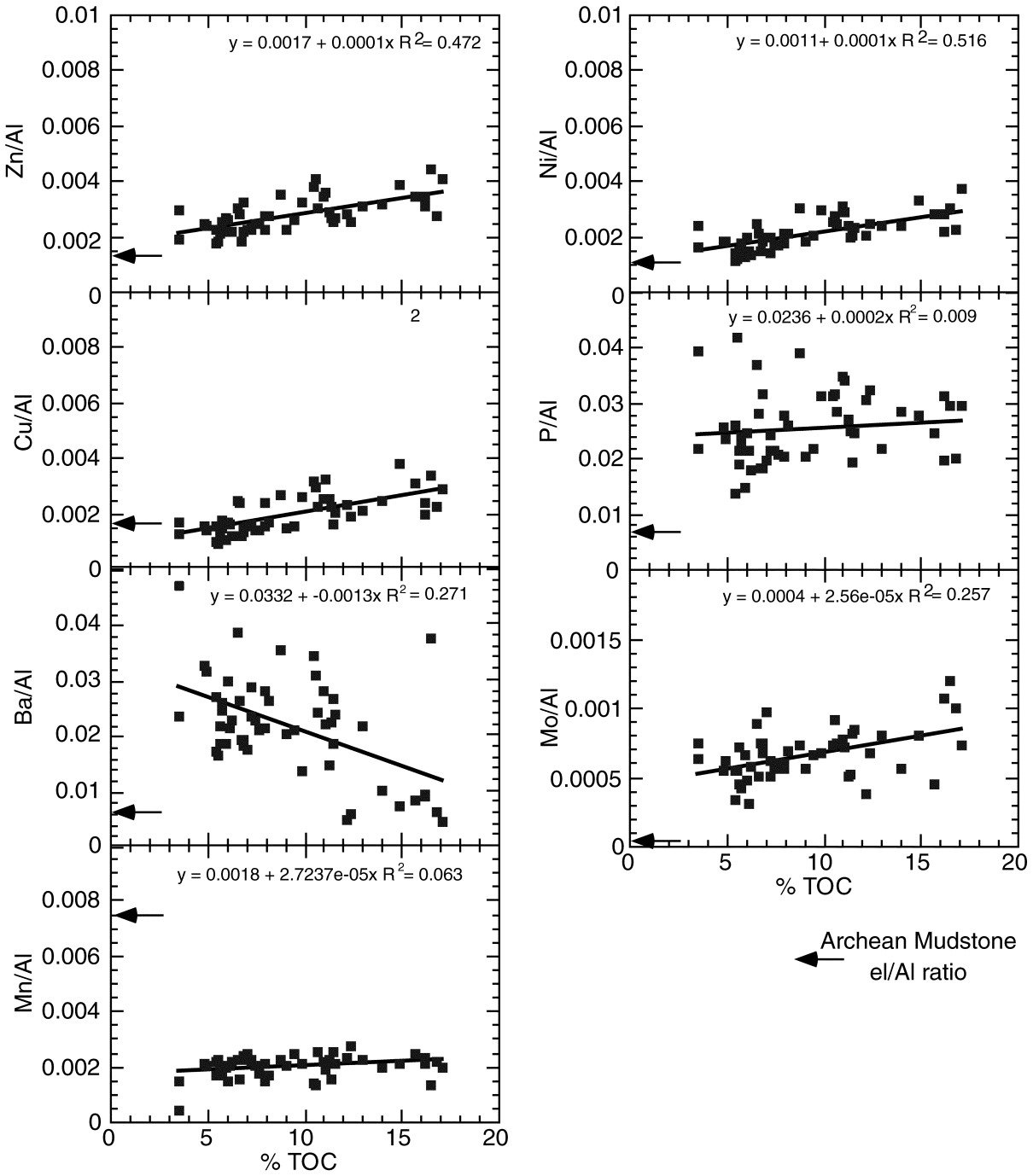

Fig. 9. Plots of element/Al ratios versus % TOC demonstrate trace element enrichments relative to lithogenic contributions and assess their relationship to TOC. Element/Al values for Archean Mudstone (Taylor and McLennan, 1985), an approximation of the terrigenous source composition for these sediment, are marked by an arrow on the element/Al axis.

upwelling and thus the supply of nutrients, then export production must have changed in order to maintain the stable degree of relative nutrient utilization.

Important differences exist between the two study sites. The overall higher TOC and opal concentrations at Site 1084 probably reflect greater primary productivity because of the location of the site relative to the Lüderitz upwelling cell. The 1.1 Ma interval from Site 1084 contains higher $\delta^{13}C_{org}$ and $\delta^{15}N_{tot}$ values and the highest TOC and opal concentrations, suggesting that productivity was even higher at the time of deposition of this light–dark sequence than during either of the younger intervals studied. The increase in the extent of nitrate utilization at this time may indicate that delivery of some other limiting nutrient was greater at 1.1 Ma than around 0.7 Ma.

The trace element results suggest that organic carbon recycling regulated the seafloor geochemistry. There are obvious systematic relationships between TOC and those elements delivered primarily by organic matter and those that precipitate/dissolve under reducing conditions. Both the shipboard faunal analysis (Wefer et al., 1998) and a more detailed study of the organic carbon-rich layers (Brüchert et al., 2000) indicate that the organic carbon-rich intervals contain primarily types of benthic forams considered to be tolerant of low oxygenation conditions. Organic matter is the main reducing agent in sediment. Hence, it follows that increased input of organic matter is responsible for the depletion of the bottom water oxygen required for the in situ enrichment of Mo and the remobilization of Ba and Mn from the surface sediment.

Ba is not suitable for use as a productivity proxy in this setting because of its susceptibility to chemical remobilization under sulfate-reducing conditions. There seems to be a threshold condition that must be met before Ba loss occurs. Barite dissolution requires either high organic matter oxidation rates (McManus et al., 1998) or sulfate reduction and depletion in the pore water. Mo scavenging requires elevated concentrations of HS^- although Mo can be enriched without the loss of Ba. Sulfate reduction proceeded without barite dissolution until the sediment was buried below the depth of seawater diffusion and the pore water sulfate concentrations were low enough to initiate barite dissolution. The relationship between Mo enrichment and Ba loss appears to be another indicator of the extent/intensity of redox conditions.

Other elements associated with organic matter delivery, such as P, Ni, Zn, and Cu, are enriched above crustal values but do not show the strong associations with organic matter delivery, either as an original depositional feature or as a diagenetic feature. Thus, they cannot be readily used as paleoproductivity proxies. This limitation is likely because these elements are susceptible to diagenesis under even mildly reducing conditions.

Finally, the strong Mo enrichment at Sites 1082 and 1084 suggests that organic matter delivery drove microbial consumption of O_2 faster than the Mo-bearing seawater could replace it. Increased organic matter oxidation must have led to sulfate-reducing conditions near or at the interface with oxygenated bottom waters.

4. Conclusions

Monotonous organic carbon and nitrogen isotope compositions indicate that relative nutrient utilization did not vary across light–dark sediment intervals containing high amplitude fluctuations in organic carbon concentrations at ODP Sites 1082 and 1084 off Namibia. This observation implies that increased upwelling in the region led to a proportional increase in export production. An offset in the isotope measurements between Sites 1082 and 1084 mimics the spatial distribution of $\delta^{15}N_{tot}$ described by Holmes et al. (1998) in a modern study of the region. At present the Lüderitz region (Site 1084) has higher export productivity and heavier isotope values than the northern Cape Basin (Site 1082), and we infer a similar situation in the Pleistocene.

Mn/Al, P/Al, Ba/Al, and Mo/Al data provide information about organic matter oxidation in the sediments. Ba/Al profiles indicate dissolution of barite during diagenesis due to undersaturation of sulfate induced by the oxidation of organic matter. The coincidence of high % TOC, low

Ba/Al, high Mo, and slight enrichments of Cu, Ni, and Zn, along with low Mn/Al values imply that delivery and oxidation of organic matter are intrinsically linked. We conclude that variations in the inorganic trace metal compositions of sediment are fundamentally related to export productivity in the BCUS.

We conclude that changes in productivity led to the generation of the color cycles. Dark intervals represent times of enhanced productivity and delivery of oxidizable organic carbon to the seafloor leading to the enrichment of metals and dissolution of carbonate. The light, relatively carbonate-rich intervals are generated when organic carbon delivery is lower.

Acknowledgements

We are grateful to Margaret Lansing and Brian Eadie for making possible the stable isotope analyses at the NOAA Great Lakes Environmental Research Laboratory in Ann Arbor, MI. Thanks to T.J. Shaw and W. Dean for their comments on an earlier version of this contribution. We thank Tom Pedersen and an anonymous reviewer for their constructive reviews. P.A.M. thanks the Deep Sea Drilling Project and the Ocean Drilling Program, funded by the National Science Foundation and IPOD countries, for providing the unique opportunity to participate in both Leg 75 and Leg 175. This study was supported by funds from JOI-USSSP to P.A.M. and R.W.M. Trace metal analyses at Boston University supported by NSF EAR-9724282.

References

Altabet, M.A., Francois, R., 1994. Sedimentary nitrogen isotopic ratio as a recorder for surface nitrate utilization. Global Biogeochem. Cycles 8, 103–116.

Altabet, M.A., Francois, R., Murray, D.E., Prell, W.L., 1995. Climate-related variations in denitrification in the Arabian Sea from sediment $^{15}N/^{14}N$ ratios. Nature 373, 506–509.

Altabet, M.A., Pilskaln, C., Thunell, R., Pride, C., Sigman, D., Chavez, F., Francois, R., 1999. The nitrogen isotope biogeochemistry of sinking particles from the margin of the Eastern North Pacific. Deep-Sea Res. 46, 655–679.

Berger, W.H., 1970. Biogenous deep-sea sediments: Fractionation by deep-sea circulation. Geol. Soc. Am. Bull. 81, 1385–1402.

Berger, W.H., Wefer, G., Richter, C., Lange, C.B., Giraudeau, J., Hermelin, O., Party, S.S., 1998. The Angola–Benguela Upwelling System: Paleoceanographic synthesis of shipboard results from Leg 175. In: Wefer, G., Berger, W.H., Richter, C. et al. (Eds.), Proceedings of the Ocean Drilling Program Initial Reports. Ocean Drilling Program, College Station, TX, pp. 505–531.

Bertrand, P., Pedersen, T.F., Martinez, P., Calvert, S., Shimmield, G., 2000. Sea level impact on nutrient cycling in coastal upwelling areas during deglaciation: Evidence from nitrogen isotopes. Global Biogeochem. Cycles 14, 341–355.

Brandes, J.A., Devol, A.H., Yoshinare, T., Jayakumar, D.A., Naqvi, S.W.A., 1998. Isotopic composition of nitrate in the central Arabian Sea and eastern tropical North Pacific: A tracer for mixing and nitrogen cycles. Limnol. Oceanogr. 43, 1680–1689.

Broecker, W., 1982. Ocean chemistry during glacial time. Geochim. Cosmochim. Acta 46, 1689–1705.

Brüchert, V., Perez, M.E., Lange, C.B., Giradeau, J., Hermelin, O., Party, S.S., 2000. Coupled primary production, benthic foraminferal assemblage, and sulfur diagenesis in organic-rich sediments of the Benguela upwelling system. Mar. Geol. 163, 27–40.

Brumsack, H.J., 1986. The inorganic geochemistry of Cretaceous black shales (DSDP Leg 41) in comparison to modern upwelling sediments from the Gulf of California. In: Summerhayes, C.P., Shackleton, N.J. (Eds.), North Atlantic Palaeoceanography. Geological Society of America, pp. 447–462.

Calvert, S.E., Pedersen, T.F., 1994. Sedimentary geochemistry of manganese: Implications for the environment of formation of manganiferous black shales. Econ. Geol. 91, 36–47.

Calvert, S.E., Price, N.B., 1970. Minor metal contents of recent organic-rich sediments off South West Africa. Nature 227, 593–595.

Collier, R., Edmond, J., 1984. The trace element geochemistry of marine biogenic particulate matter. Prog. Oceanogr. 13, 113–199.

Crusius, J., Calvert, S., Pedersen, T., Sage, D., 1996. Rhenium and molybdenum enrichments in sediments as indicators of oxic, suboxic, and sulfidic conditions of deposition. Earth Planet. Sci. Lett. 145, 65–78.

Degens, E.T., Mopper, K., 1976. Factors controlling the distribution and early diagenesis of organic material in marine sediments. In: Riley, J.P., Chester, R. (Eds.), Chemical Oceanography, pp. 60–113.

Dickens, G.R., Owen, R.M., 1994. Late Miocene–early Pliocene manganese redirection in the central Indian Ocean: Expansion of the intermediate water oxygen minimum zone. Paleoceanography 9, 169–181.

Diester-Haass, L., Meyers, P.A., Rothe, P., 1986. Light–dark cycles in opal-rich sediments near the Plio-Pleistocene boundary DSDP Leg 75, Site 532 m Walvis Ridge Continental Terrace. Mar. Geol. 73, 1–23.

Dymond, J., Suess, E., Lyle, M., 1992. Barium in deep-sea sediment: A geochemical proxy for paleoproductivity. Paleoceanography 7, 163–181.

Emerson, S., Bender, M.L., 1981. Carbon fluxes at the sediment–water interface of the deep sea: calcium carbonate preservation. J. Mar. Res. 39, 139–162.

Emerson, S., Hedges, J.I., 1988. Processes controlling the organic carbon content of open ocean sediments. Paleoceanography 3, 621–634.

Erickson, B.E., Helz, G.R., 2000. Molybdenum (VI) speciation in sulfidic waters: Stability and lability of thiomolybdates. Geochim. Cosmochim. Acta 64, 1149–1158.

Francois, R., 1988. A study on the regulation of the concentrations of some trace metals (Rb, Sr, Zn, Pb, Cu, V, Cr, Ni, Mn, and Mo) in Saanich Inlet sediments, British Columbia, Canada. Mar. Geol. 83, 285–308.

Francois, R., Altabet, M.A., Burckle, L.H., 1992. Glacial to interglacial changes in surface nitrate utilization in the Indian sector of the Southern Ocean as recorded by sediment $\delta^{15}N$. Paleoceanography 7, 589–606.

Ganeshram, R.S., Pedersen, T.F., Calvert, S.E., Murray, J.W., 1995. Large changes in oceanic nutrient inventories from glacial to interglacial periods. Nature 376, 755–757.

Ganeshram, R.S., Calvert, S.E., Pedersen, T.F., Cowie, G.L., 1999. Factors controlling the burial of organic carbon in laminated and bioturbated sediments off NW Mexico: Implications for hydrocarbon preservation. Geochim. Cosmochim. Acta 63, 1723–1734.

Ganeshram, R.S., Pedersen, T.F., Calvert, S.E., McNeill, G.W., Fontugne, M.R., 2000. Glacial–interglacial variability in denitrification in the world's oceans: Causes and consequences. Paleoceanography 15, 361–376.

Gardner, J.V., Dean, W.E., Wilson, C.R., 1984. Carbonate and organic-carbon cycles and the history of upwelling at Deep Sea Drilling Project Site 532, Walvis Ridge, South Atlantic Ocean. In: Hay, W.W., Sibuet, J.-C. et al. (Eds.), Initial Reports DSDP. U.S. Govt. Printing Office, Washington, DC, pp. 905–953.

Hammond, D.E., Giordani, P., Berelson, W.M., Poletti, R., 1999. Diagenesis of carbon and nutrients and benthic exchange in sediments of the Northern Adriatic Sea. Mar. Chem. 66, 53–79.

Haug, G.H., Pedersen, T.F., Sigman, D.M., Calvert, S.E., Nielsen, B., Peterson, L.C., 1998. Glacial/interglacial variations in production and nitrogen fixation in the Cariaco Basin during the last 580 kyr. Paleoceanography 13, 427–432.

Helz, G.R., Miller, C.V., Charnock, J.M., Mosselmans, J.F.W., Pattrick, R.A.D., Garner, C.D., Vaughan, D.J., 1996. Mechanism of molybdenum removal from the sea and its concentration in black shales: EXAFS evidence. Geochim. Cosmochim. Acta 60, 3631–3642.

Holmes, M.E., Müller, P.J., Schneider, R.R., Segl, M., Pätzold, J., Wefer, G., 1996. Stable isotopes in Angola Basin surface sediments. Mar. Geol. 134, 1–12.

Holmes, M.E., Müller, P.J., Schneider, R.R., Segl, M., Wefer, G., 1998. Spatial variations in euphotic zone nitrate utilization based on $\delta^{15}N$ in surface sediments. GeoMar. Lett. 18, 58–65.

Ingall, E., Jahnke, R., 1994. Evidence for enhanced phosphorus regeneration from marine sediments overlain by oxygen depleted waters. Geochim. Cosmochim. Acta 58, 2571–2575.

Kienast, M., 2000. Unchanged nitrogen isotopic composition of organic matter in the South China Sea during the last glacial cycle: Global implications. Paleoceanography 15, 244–253.

Lange, C.B., Berger, W.H., Lin, H.-L., Wefer, G., 175, S.S.P.L., 1999. The early Matuyama Diatom Maximum off SW Africa, Benguela Current System (ODP Leg 175). Mar. Geol. 161, 93–114.

Leinen, M., Cweink, D., Biscaye, P.E., Heath, G.H., Kolla, V., Thiede, J., Dauphin, J., 1986. Distribution of biogenic silica and quartz in recent deep sea sediments. Geology 14, 199–203.

Liu, K.-K., Kaplan, I.R., 1989. The eastern tropical Pacific as a source of 15N-enriched nitrate in seawater off southern California. Limnol. Oceanogr. 34, 820–830.

Lutjeharms, J.R.E., Meeuwis, J.M., 1987. The extent and variability of south-east Atlantic upwelling. S. Afr. J. Mar. Sci. 5, 51–62.

Lutjeharms, J.R.E., Stockton, P.L., 1987. Kinematics of the upwelling of southern Africa. S. Afr. J. Mar. Sci. 5, 35–49.

Lyle, M., Murray, D.W., Finney, B.P., Dymond, J., Robbins, J.M., Brooksforce, K., 1988. The record of late Pleistocene biogenic sedimentation in the eastern tropical Pacific Ocean. Paleoceanography 3, 39–59.

McIver, R.D., 1975. Hydrocarbon occurrences from JOIDES Deep Sea Drilling Project. Proceedings, World Petroleum Congress 9, 2 (Geology), pp. 269–280.

McManus, J., Berelson, W.M., Coale, K.H., Johnson, K.S., Kilgore, T.E., 1997. Phosphorus regeneration in continental margin sediments. Geochim. Cosmochim. Acta 61, 2891–2907.

McManus, J., Berelson, W.M., Klinkhammer, G.P., Johnson, K.H., Anderson, R.F., Kumar, N., Burdige, D., Hammond, D.E., Brumsack, H.J., McCorckle, D.C., Rushdi, A., 1998. Geochemistry of barium in marine sediments: Implications for its use as a paleoproxy. Geochim. Cosmochim. Acta 62, 2453–2473.

Meyers, P.A., 1984. Organic geochemistry of sediments from the Angola Basin and the Walvis Ridge: A synthesis of studies from Deep Sea Drilling Project Leg 75. In: Hay, W.W., Sibuet, J.-C. et al. (Eds.), Initial Reports DSDP. U.S. Govt. Printing Office, Washington, DC, pp. 459–467.

Meyers, P.A., 1994. Preservation of elemental and isotopic source identification of sedimentary organic matter. Chem. Geol. 114, 289–302.

Meyers, P.A., 1997. Organic geochemical proxies of paleoceanographic, paleolimnologic, and paleoclimatic processes. Org. Geochem. 27, 213–250.

Meyers, P.A., Doose, H., 1999. Sources, preservation, and thermal maturity of organic matter in Pliocene–Pleistocene organic-carbon-rich sediments of the western Mediterranean Sea. In: Zahn, R., Comas, M.C., Klaus, A. (Eds.), Proceed-

ings of the Ocean Drilling Program, Scientific Results. Ocean Drilling Program, College Station, TX.

Morford, J.L., Emerson, S., 1999. The geochemistry of redox sensitive trace metals in sediments. Geochim. Cosmochim. Acta 63, 1735–1750.

Mortlock, R.A., Froelich, P.N., 1989. A simple method for the rapid determination of biogenic opal in pelagic marine sediments. Deep-Sea Res. 36, 1415–1426.

Müller, G., Gastner, M., 1971. The 'karbonate bomb', a simple device for determination of carbonate content in sediments, soils, and other materials. N. Jahrb. Mineral. 10, 446–469.

Müller, P.J., Suess, E., 1979. Productivity, sedimentation rate and seidmentary organic matter in the oceans. I. Organic matter preservation. Deep-Sea Res. 26, 1347–1362.

Murray, R.W., Leinan, M., Isern, A.R., 1993. Biogenic flux of Al to sediment in the central equatorial Pacific Ocean: Evidence for increased productivity during the glacial periods. Paleoceangraphy 8, 651–670.

Murray, R.W., Leinen, M., 1996. Scavenged excess aluminum and its relationship to bulk titanium in biogenic sediment from the central equatorial Pacific Ocean. Geochim. Cosmochim. Acta 60, 3869–3878.

Nijenhuis, I.A., Lange, G.J.D., 2000. Geochemical constraints on Pliocene sapropel formation in the eastern Mediterranean. Mar. Geol. 163, 41–63.

Piper, D.V., Isaacs, C.M., 1995. Minor elements in Quaternary sediment from the Sea of Japan: A record of surface-water productivity and intermediate-water redox conditions. GSA Bull. 107, 54–67.

Rau, G.H., Arthur, M.A., Dean, W.E., 1987. $^{15}N/^{14}N$ variations in Cretaceous Atlantic sedimentary sequences: implication for past changes in marine nitrogen biogeochemistry. Earth Planet. Sci. Lett. 82, 269–279.

Rea, D.K., Pisias, N.G., Newberry, T., 1991. Late Pleistocene paleoclimatology of the central equatorial Pacific: Flux pattern of biogenic sediments. Paleoceanography 6, 227–244.

Sachs, J., Repeta, D., 1999. Oligotrophy and nitrogen fixation during eastern Mediterranean sapropel events. Science 286, 2485–2488.

Sarnthein, M., Winn, K., Duplessy, J.-C., Fontugne, M.R., 1988. Global variations of surface water productivity in low- and mid-latitudes: influence on CO_2 reservoirs of the deep ocean and atmosphere during the last 21,000 years. Paleoceanography 3, 361–399.

Schroeder, J.O., Murray, R.W., Leinen, M., Pflaum, R.C., Janecek, T.R., 1997. Barium in equatorial Pacific carbonate sediment: Terrigenous, oxide, and biogenic associations. Paleoceanography 12, 125–146.

Seisser, W.G., 1980. Late Miocene origin of the Benguela upwelling system off northern Namibia. Science 208, 125–146.

Stein, R., Haven, H.L.T., Littke, R., Rullkotter, J., Welte, D.H., 1989. Accumulation of marine and terrigenous organic carbon at upwelling Site 658 and nonupwelling Sites 657 and 659: Implications for reconstruction of paleoenvironments in the eastern subtropical Atlantic through the late Cenozoic times. In: Ruddiman, W.F., Sarnthein, M. et al. (Eds.), Proceedings of the Ocean Drilling Program, Scientific Results. Ocean Drilling Program, College Station, TX, pp. 361–386.

Summerhayes, C.P., Kroon, D., Rosell, M.A., Jordan, R.W., Schrader, H.J., Hearn, R., Villanueva, J., Grimalt, J.O., Eglinton, G., 1995. Variability in the Benguela Current upwelling system. Prog. Oceanogr. 35, 207–251.

Taylor, S.R., McLennan, S.M., 1985. The Continental Crust: Its Composition and Evolution. Blackwell, Oxford, 312 pp.

Thamdrup, B., Gludl, R.N., Hansen, J.W., 1994. Manganese oxidation and in situ manganese fluxes. Geochim. Cosmochim. Acta 58, 2563–2570.

Verardo, D.J., McIntyre, A., 1994. Production and destruction: Control of biogenous sedimentation in the tropical Atlantic 0–300,000 years B.P. Paleoceanography 9, 63–86.

Wefer, G., Berger, W.H., Richter, C., et al., 1998. Introduction: Background, scientific objectives and principal results for Leg 175 (Benguela Current and the Angola–Benguela upwelling systems). In: Wefer, G., Berger, W.H., Richter, C. et al. (Eds.), Proceedings of the Ocean Drilling Program Initial Reports. Ocean Drilling Program, College Station, TX.

Yarincik, K.M., Murray, R.W., Peterson, L.C., 2000a. Climatically controlled eolian and hemipelagic deposition in the Carioco Basin, Venezuela, over the past 578,000 years: Results from Al/Ti and K/Al. Paleoceanography 15, 210–228.

Yarincik, K.M., Murray, R.W., Peterson, L.C., Haug, G.H., 2000b. Oxygenation history of bottom waters in the Cariaco Basin, Venezuela, over the past 578,000 years: Results from redox sensitive metals (Mo, V, Mn, Fe). Paleoceanography 15, 593–604.